GSA Data Repository 2019226

Caudron, C., et al., 2019, Change in seismic attenuation as a long-term precursor of gas-driven eruptions: Geology, https://doi.org/10.1130/G46107.1

APPENDICES

Methods

Seismic data from Ruapehu and Tongariro were downloaded from GNS (https://www.geonet.org.nz/) while Kawah Ijen data were acquired through a cooperation between the Royal Observatory of Belgium, Center of Volcanology and Geological Hazard Mitigation and U.S Geological Survey. The 1-day vertical seismic displacements were automatically detrended and high-passed filtered (above 0.5 Hz to avoid the oceanic contamination). The daily signal was filtered (4 corners, butterworth) in two frequency bands, 4.5-8 Hz and 8-16 Hz, and then sliced into 10-minute segments. The absolute amplitudes were computed and the ratio between low and high frequencies exported. The median was computed every day along with its uncertainty using a bootstrap procedure with 1000 random samples. The bootstrap estimate exported the values for 95% confidence interval.

The 1-day results were smoothed using rolling median of 2 years for Ruapehu and Tongariro (day of interest plus the 729 days preceding), whereas only 90 days (day of interest plus the 89 days preceding) for the shorter timeseries of Kawah Ijen. Different number of days did not change the shape of the overall curve and the long-term behaviour, but slightly shifted the maxima (Supplemental information Figure S3). Smaller number of days at New Zealand volcanoes were too noisy, whereas, the time series acquired at the Kawah Ijen volcano was too short to apply a 2-year moving window. Note that the instrument response was not systematically deconvolved for each seismic station because it dramatically increased the computation time without changing the results (Supplemental information Figure S4), and instrument responses are usually stable over time.

Model

Shallow tremor at the target volcanoes is assumed to arise from the pressure oscillations ΔP that emerge spontaneously in gas cavities trapped beneath permeable media (e.g., shallow volcanic cap or edifice), as proposed by Girona et al. (2019; in review). These pressure oscillations emerge in response to three concurrent processes: the permeable flow of gases through the shallow cap, the temporary accumulation of gases beneath the permeable cap, and the persistent supply of volatiles from deeper levels. By convolving these pressure oscillations ΔP with the Green's function describing the propagation of Rayleigh waves along the shallow crust (i.e.,

from the source to the receiver), Girona et al. (2019; in review) found that the vertical ground displacement u_z recorded at nearby stations is given, in the frequency domain, by:

$$u_z(\omega) = \left[S\frac{\sum_{l=0}^{\infty}\gamma_l(j\omega)^l}{\sum_{l=0}^{\infty}\Gamma_l(j\omega)^l}\right]\left[\sum_{k=1}^{N} q_k e^{-j\omega t_k}\right]\left[\sqrt{\frac{2v_c\omega}{\pi r}}\frac{e^{-\frac{\omega r}{2v_u Q_f}}}{8\rho_s v_c^2 v_u}\; e^{j\left(\frac{\omega r}{v_c}+\frac{\pi}{4}\right)}\right] \quad , \qquad (1)$$

where S is the cross-sectional area of the permeable cap (the same as the cross-sectional area of the gas cavity), j is the imaginary unit, ω is the angular frequency, q_k is the mass of gas supplied to the gas pocket at the instant t_k, N is the total number of mass impulses in the gas pocket during a given simulation time, v_c is the phase velocity (we use $v_c = 1295(\omega/2\pi)^{-0.374}$ m/s), r is the distance from the source to the receiver, v_u is the group velocity, Q_f is the dimensionless quality factor, ρ_s is the density of the medium through which seismic waves propagate (i.e., crust), and γ_l and Γ_l are coefficients that depend on different physical and geometrical parameters of the model. For the case of thin (<100 m) and highly permeable caps ($\sim 10^{-10} - 10^{-7}$; realistic for caps and shallow volcanic edifices; Jaupart and Allègre, (1991)), which means tremor originated at shallow levels beneath active craters, equation (1) simplifies to (see details in Girona et al., 2019 in review):

$$u_z(\omega) = \left[S\frac{\gamma_0 + j\gamma_1\omega}{\Gamma_0 - \Gamma_2\omega^2 + j\Gamma_1\omega}\right]\left[\sum_{k=1}^{N} q_k e^{-j\omega t_k}\right]\left[\sqrt{\frac{2v_c\omega}{\pi r}}\frac{e^{-\frac{\omega r}{2v_u Q_f}}}{8\rho_s v_c^2 v_u}\; e^{j\left(\frac{\omega r}{v_c}+\frac{\pi}{4}\right)}\right] \quad . \qquad (2)$$

In this case, the parameters γ_0, γ_1, Γ_0, Γ_1, and Γ_2 are defined as $\gamma_0 = \frac{\beta_b L}{\beta_a}$, $\gamma_1 = \frac{\beta_c L}{\beta_a}$, $\Gamma_0 = 1$, $\Gamma_1 = [2(\beta_a\beta_d + \beta_b\beta_e)L + \beta_a\beta_b L^2]/2\beta_a$, and $\Gamma_2 = [2\beta_c\beta_e L + \beta_a\beta_c L^2]/2\beta_a$. In turn, $\beta_a = \frac{S\varphi M}{R_g T}$; $\beta_b = \frac{\mu\varphi}{\kappa\left(P_{ex} - \frac{R_g T Q_0^2}{S^2\varphi^2 M P_{ex}}\right)}$; $\beta_c = \frac{P_{ex} M}{R_g T\left(P_{ex} - \frac{R_g T Q_0^2}{S^2\varphi^2 M P_{ex}}\right)}$; $\beta_d = \frac{2Q_0}{S\varphi\left(P_{ex} - \frac{R_g T Q_0^2}{S^2\varphi^2 M P_{ex}}\right)}$; and $\beta_e = \frac{SMD}{R_g T}$, where μ is the gas viscosity; φ and κ are the cap porosity and permeability, respectively; P_{ex} is the pressure at the exit vent (i.e., atmospheric/hydrostatic pressure for volcanoes without/with crater lake); R_g is the ideal gas constant; T is the gas temperature (assumed to be constant in tremor timescales); Q_0 is the mean outgassing flux; M is the molecular weight of volcanic/hydrothermal gases (mostly water vapor); and L is the thickness of the cap. The ground displacement described by equation (2) can explain the main features of shallow volcanic seismicity (Girona et al., 2019), particularly monochromatic and broadband tremor as typically recorded around Kawah-Ijen, Ruapehu, and Tongariro volcanoes. In our study, we use equation (2) to generate synthetic seismograms for different values of the seismic quality factor Q_f at different source-receiver distances; note that decreasing values of Q_f represents increasing

values of seismic attenuation. Then, we calculate DSAR following an approach similar to the analysis performed with the natural data.

In particular, the values of the model parameters used in our simulations are as follows: cross-sectional area of the permeable cap $S = 1{,}500\ \mathrm{m}^2$ (equivalent to a cylindrical cap with radius ~22 m), cap thickness $L = 50$ m, cap permeability $\kappa = 10^{-8}$ m^2, cap porosity $\varphi = 0.1\%$ (porous flow assumed to be controlled by fractures and open channels of the cap), mean outgassing flux $Q_0 = 2$ kg/s, gas cavity thickness $D = 10$ cm, external pressure $P_{ex} = 1$ atm, gas temperature $T = 1{,}000$ ℃, gas viscosity $\mu_g = 10^{-5}$ Pa s, and molecular weight of gas (mostly water vapour) $M = 0.018$ kg/mol. We also use distance source-station $r = 600$ m, 1500 m and 3,800 m, density of the medium (i.e., density of the crust, through which seismic waves propagate from the source to the receiver) $\rho_s = 3{,}000$ kg/m^3, frequency-dependent phase velocity $v_c = 1295(\omega/2\pi)^{-0.374}$ m/s, group velocity $v_u = 0.73 v_c$, and quality factor in the range $Q_f = 10 - 200$. We impose the random bursting of $N = 1{,}000$ bubbles in 50 s of simulation. These values of the parameters allow generating synthetic seismicity with dominant frequencies below ~3 Hz band, as observed in Ruapehu, Kawah Ijen, and Tongariro. Details on the calculation of the vertical ground displacement u_z can be found in Girona et al. (2019, in review).

Possible Modulators of Activity for Each Volcano

Kawah Ijen

Regional earthquakes (magnitude in parentheses (M_w), source: USGS earthquake catalogue, https://earthquake.usgs.gov/earthquakes/search/):

- Banda Sea, Indonesia 2012/12/10 (7.1)
- Enarotali, Indonesia 2013/4/6 (7.0)
- Gasbayan, Philippines 2013/10/15 (7.1)
- Ternate, Indonesia 2014/11/15 (7.8)
- Nebe, Indonesia 2015/2/27 (7.0)
- Abepura, Indonesia 2015/7/27 (7.0)
- Sumatra, Indonesia 2016/3/2 (7.8)
- Agrihan, Mariana Islands 2016/7/29 (7.7)

Nearby earthquake swarm (source: USGS earthquake catalog: https://earthquake.usgs.gov/earthquakes/search/) and volcano eruption:

- South of Java earthquake swarm, Indonesia 2012/9/4 to 2012/9/15 (maximum M_w of 6.1 and depth ranging between 4.8 and 14 km)
- Raung volcano eruption (~20 km from Kawah Ijen, East Java, Indonesia 2015/2/1 to 2015/8/22 (VEI=3, source: Global Volcanism Program))

Atmospheric pressure and rainfall data were downloaded from the NNDC Climate Data (station located at Banyuwangi airport, East Java, Indonesia, source: https://www7.ncdc.noaa.gov/CDO/cdo).

Ruapehu and Tongariro volcanoes

Regional earthquakes (magnitude (M_w) in parentheses):

- Gisborne, New Zealand 2001/12/20 (6.7)
- Christchurch, New Zealand 2010/9/4 (7.1)
- Christchurch, New Zealand 2011/2/22 (6.3)
- Kaikoura, New Zealand 2016/11/14 (7.8)

Atmospheric pressure and rainfall data were downloaded from the National Climate Database (station located at Wanganui, Spriggens Park, New Zealand, source: https://cliflo.niwa.co.nz/).

Tongariro volcano

Repeated earthquake swarms at Ngaurauhoe volcano (~5 km from Tongariro) from 2005 to 2010 (Jolly et al., 2012).

Description of Gas-Driven Explosions

Kawah Ijen

The first gas-driven eruption analysed in this study occurred on 20 March 2013. A sudden volcanic lake temperature increase was recorded along with an equally sudden lake level increase and explosions that caused the sulfur miners to leave. The lake water temperature rose to 59°C, the highest temperature ever measured with high-resolution sensors, which had been in place since June 2010, a week after the eruption. The seismic activity was characterized by a seismic sequence reflecting an interplay between different physical sources. A very long period seismic event initiated the sequence directly followed by a seiche (i.e., an eigen-oscillation or resonance of the crater lake). A succession of high frequency bursts (>1-20 Hz) of variable durations (3 and 10 minutes) were accompanied by tilt (dominant period of 12-18 minutes) on the horizontal components of the broadband sensors. Heat and fluids discharge was abnormal until mid April 2014. This gas-driven explosion sequence was therefore characterized as major and is described in detail in Caudron et al. (2018).

The 15 May 2014 explosion was poorly monitored because the monitoring network experienced problems. Sustained upwelling of bubbles was observed in the western part of the crater lake early May 2014 (Caudron et al., 2017). When a new temperature sensor was immersed in the lake on 16 May 2014, the temperature was abnormal but never exceeded ~45°C. This gas-driven explosion was therefore characterized as minor.

A major gas-driven event occurred in October 2015 when the lake temperature reached 50°C. Simultaneously and for the first time, smoking precipitates were observed floating on the

northern part of the lake surface. These were interpreted as high temperature sulphur mats that rose from the bottom of the lake, where temperatures exceed ~100°C, directly to the surface (Caudron et al., 2015b). Bubbles can transport sulphur towards the surface (Caudron et al., 2016). A dramatic and unprecedented increase in SO_4/Cl ratio (from 2 to 5, V. van Hinsberg, pers. com.) was recorded in the acidic river at the same time. This was ascribed to an increase in the temperature of the hydrothermal system, possibly together with dissolution of previously deposited sulphate precipitates below the lake bottom (V. van Hinsberg, pers. com.). This gas-driven explosion was therefore characterized as major.

A last minor gas-driven event occurred at the end of February 2017. The lake surface became white and vigorous upwelling of bubbles were observed. The lake temperature reached 49°C. This short-lived gas-driven explosion was characterized as minor.

No other gas-driven explosion was reported nor derived from seismic data. Limnic eruptions may have occurred during rainy seasons, in April-May 2011 or January-March 2017 (Caudron et al., 2017), but were not associated with any particular seismic activity and hence seem decoupled from volcano activity.
The alert level was at 3 (on a scale of 1 to 4) between 24 July 2012 and 25 August 2013. It was decreased to 2 at 7 AM on 26 August 2013 and finally to level 1 on 8 August 2014 at 5 AM.

Ruapehu

Two gas-driven eruptions occurred at Ruapehu. The block and ash-charged 25 September 2007 explosion occurred without warning (Christenson et al., 2010). Lahars flowed in a catchment area and a ski field. The lake was relatively cold and seismically quiet (Jolly et al., 2010). This type of explosions pointed to the development of potentially hazardous conditions in the volcano during periods of quiescence and the need to understand processes operating in this system (Christenson et al., 2010). For more details, the reader is referred to Christenson et al. (2010). The 4 October 2006 explosion was much weaker and characterized as a small sub-aqueous eruption. It produced a small wave (~3 m wave height) in the Crater Lake (Jolly et al., 2010). No other volcano activity was reported. Volcanic tremor occurred in 2007-2008, as well as in April and May 2014. Some information regarding the alert levels can be found on the GVP database (https://volcano.si.edu/volcano.cfm?vn=241100).

Tongariro

Two gas-driven eruptions occurred at Tongariro and are described in Jolly et al. (2014). The 6 August 2012 eruption was the largest eruption. It severely impacted the most popular day hike in New Zealand, the Tongariro Alpine Crossing (Jolly et al., 2014a). The 21 November 2012 was smaller and only preceded by a couple of minor earthquakes (Jolly et al., 2014b). Both eruptions produced ash cloud <8 km height and pyroclastic density currents.

The precursory seismic activity prior to the first explosion consisted of three very shallow earthquake swarms on 12-13, 17-20 and 29-30 July 2012 (Hurst et al., 2014). The magmatic gas

concentrations in July 2012 had increased compared to previous measurements in May 2012. However, the seismicity did not show any accelerating trend that suggested an immediate eruption threat, indicating the difficulty of predicting small eruptions in Tongariro and similar volcanoes (Hurst et al., 2014). Some information regarding the alert levels can be found on the GVP database (https://volcano.si.edu/volcano.cfm?vn=241080).

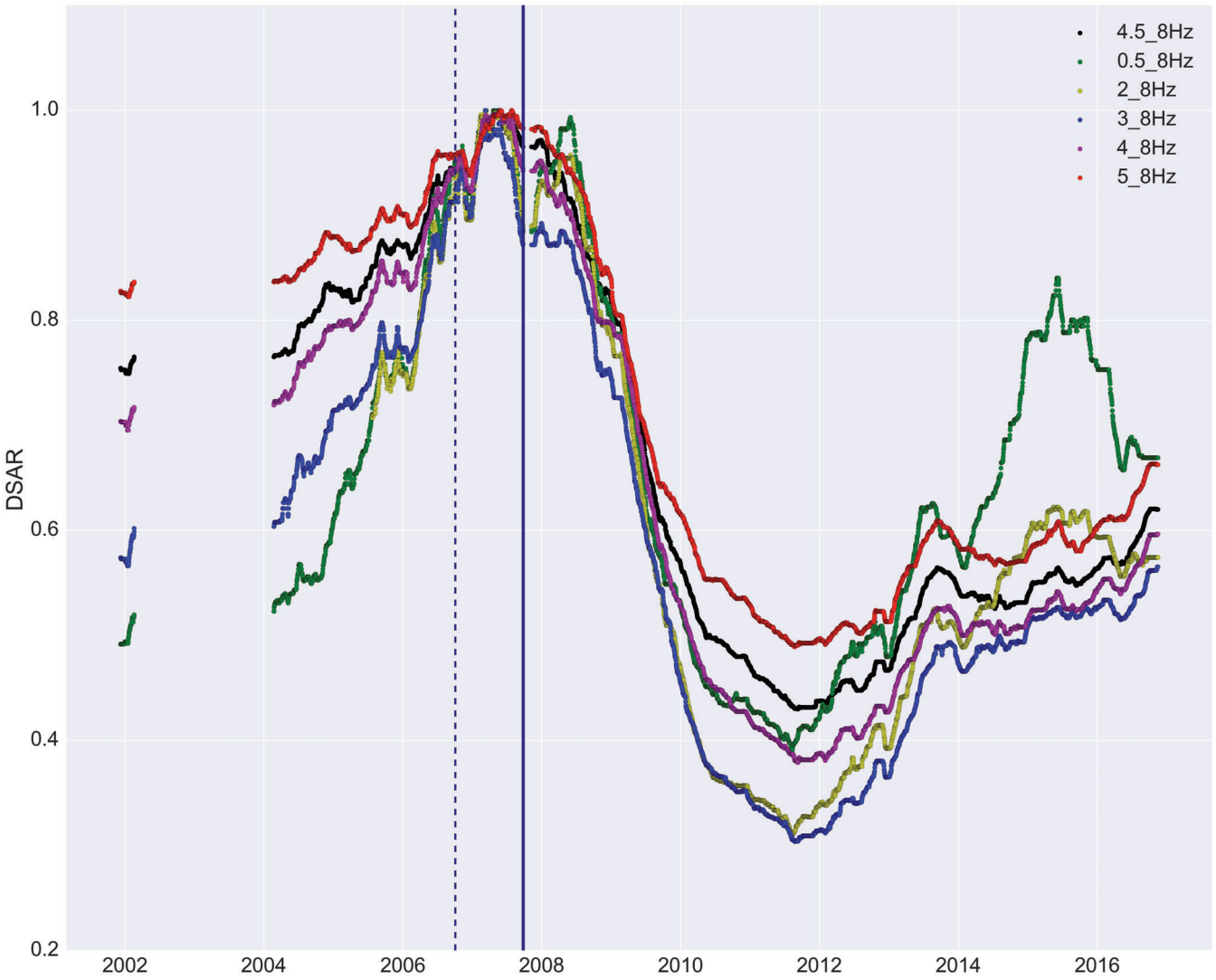

Figure DR1: DSAR results at Ruapehu depending on the lower frequency band used. The higher frequency band is always 8-16 Hz. The results are normalized for visualization purposes. A rolling median of 730 days is used as in Figure 1.

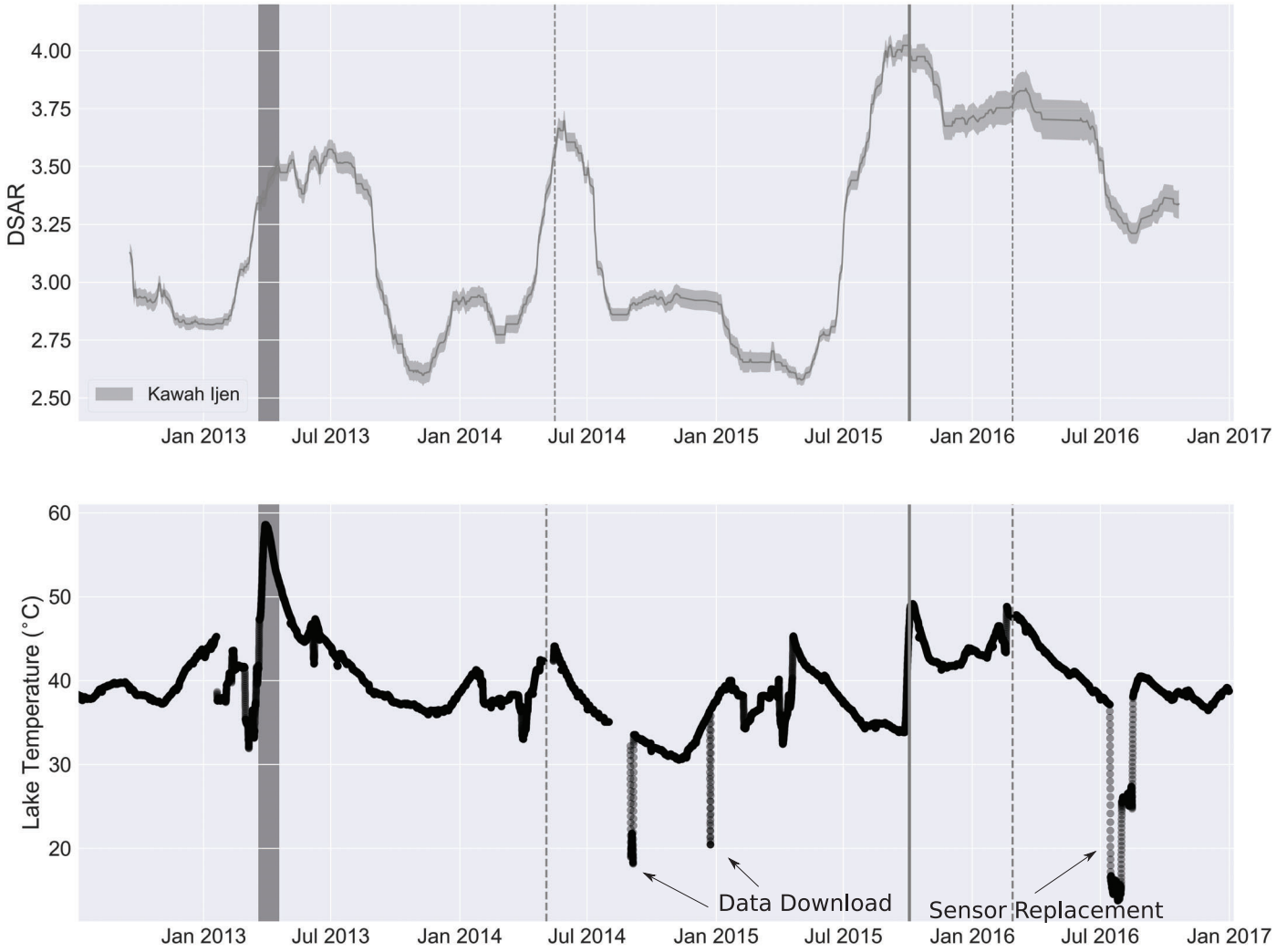

Figure DR2: comparison between DSAR and lake temperatures timeseries at Kawah Ijen. Increase in lake temperatures suggest enhanced thermal flux (Caudron et al. 2015; Lewicki et al., 2016; Caudron et al., 2017)

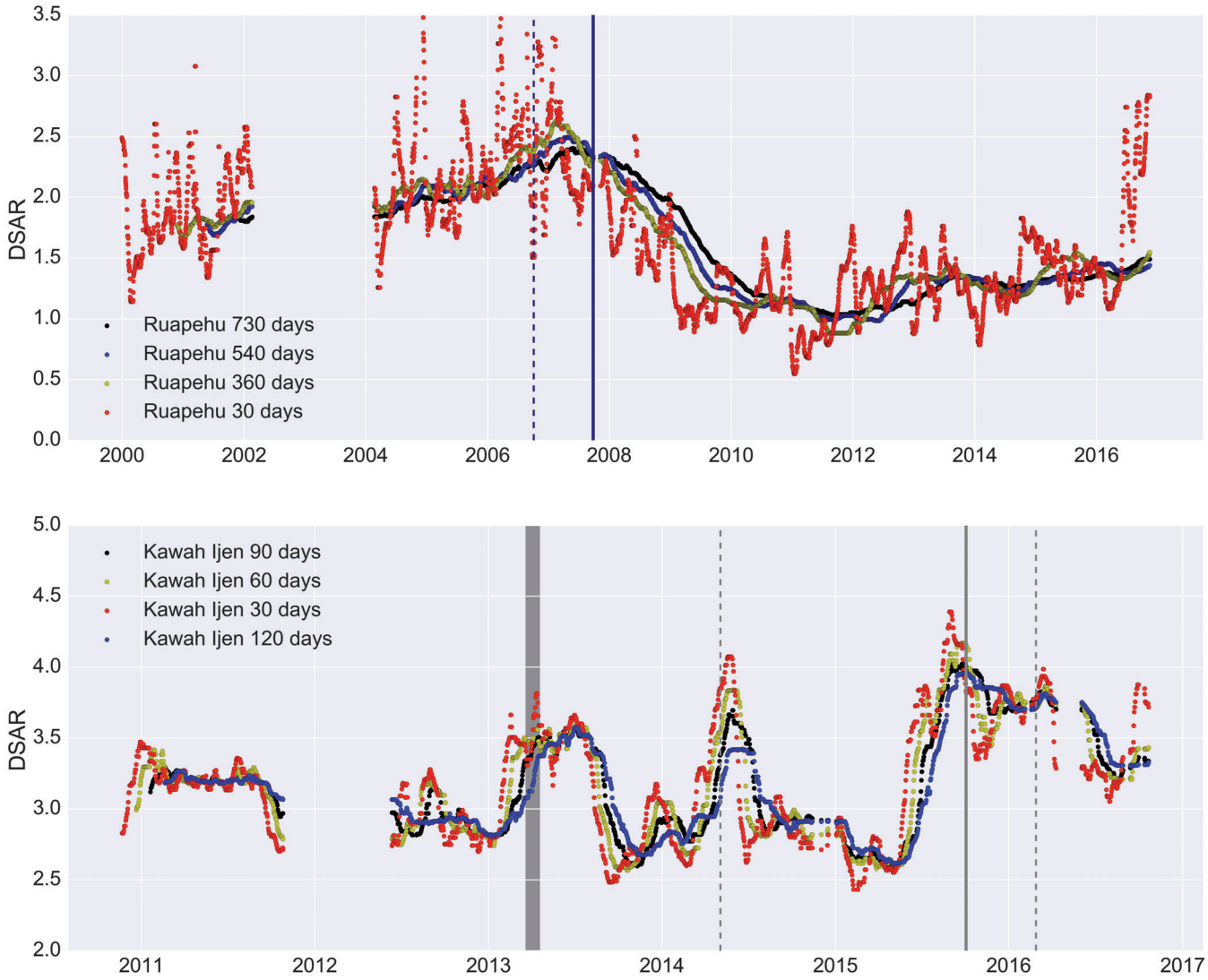

Figure DR3: DSAR results at Ruapehu and Kawah Ijen depending on different days for the moving windows (rolling median).

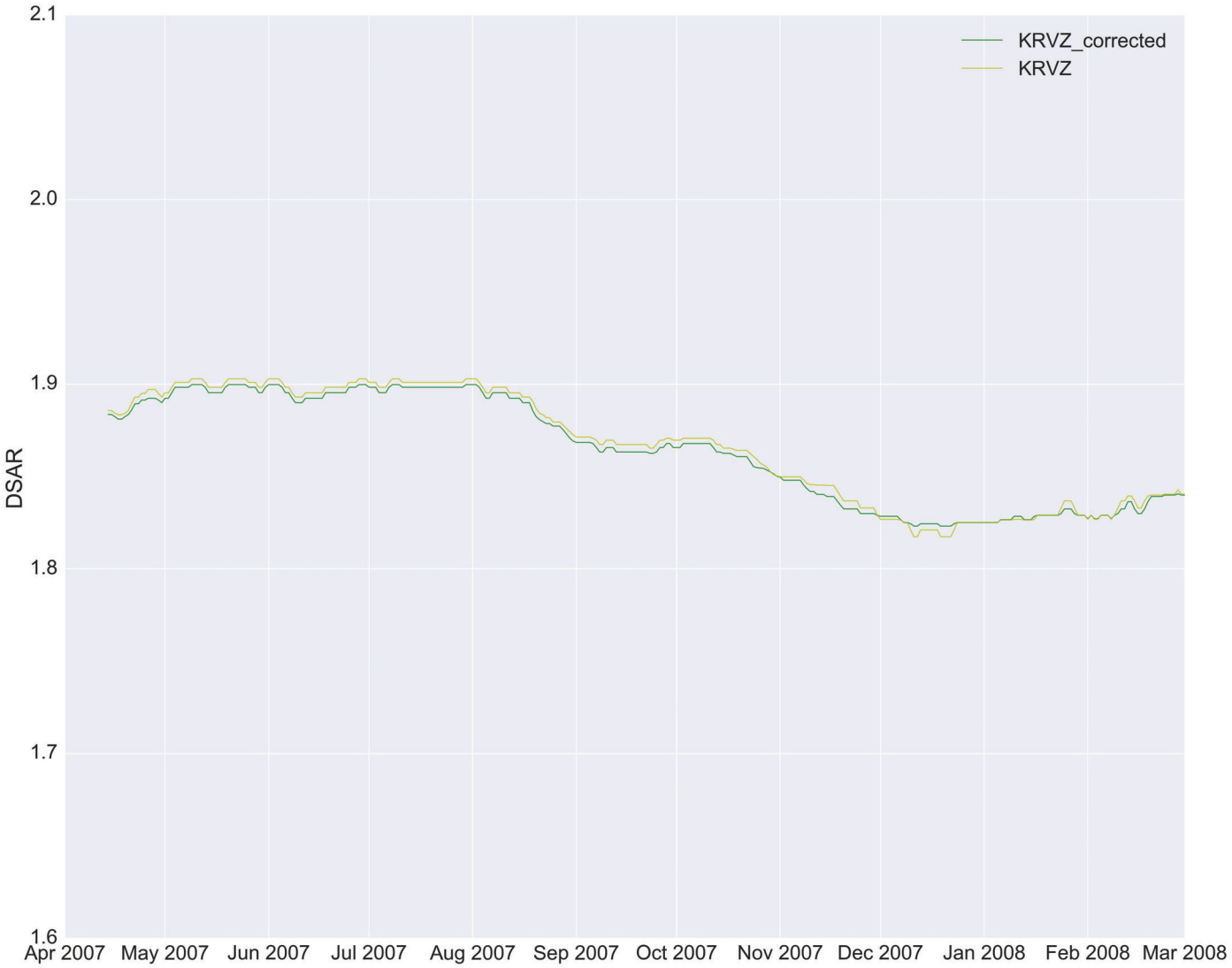

Figure DR4: difference between DSAR computed without deconvolving the instrument response (yellow line) and with deconvolution (green line). Seismic data are from station KRVZ located in Tongariro (New Zealand). A rolling median of 730 days is used as in Figure 1.

Volcano	Range
Tongariro	1-5 cm^2
Ruapehu	0.5-5 cm^2
Kawah Ijen	0.5-10 cm2

From McNutt (1992) and Benoit et al. (2003)	Range
Hydrothermal	0.05-5
Strombolian	2-30
Vulcanian/Pelean	20-150
Plinian	>100
Geysering	0.03

Table DR1: Reduced displacements calculated for each volcano. Instrument responses were deconvolved and the surface wave formula (McNutt, 1992) was used to computed reduced displacements. We now provide a range for each volcano. By inspecting the RSAM results (Figure 3) for each volcano, we extracted the largest and lowest values and calculated the corresponding RD values.